Topologically nontrivial Floquet band structure in a system undergoing photonic transitions in the ultrastrong-coupling regime

Luqi Yuan and Shanhui Fan
Department of Electrical Engineering, and Ginzton Laboratory, Stanford University, Stanford, California 94305, USA
(Received 23 April 2015; published 9 November 2015)

We consider a system of dynamically-modulated photonic resonator lattice undergoing photonic transition and show that in the ultrastrong-coupling regime such a lattice can exhibit nontrivial topological properties, including topologically nontrivial band gaps, and the associated topologically robust one-way edge states. Compared with the same system operating in the regime where the rotating wave approximation is valid, operating the system in the ultrastrong-coupling regime results in a one-way edge mode that has a larger bandwidth and is less susceptible to loss. Also, in the ultrastrong-coupling regime, the system undergoes a topological insulator-to-metal phase transition as one varies the modulation strength. This phase transition has no counterpart in systems satisfying the rotating wave approximation, and its nature is directly related to the nontrivial topology of the quasienergy space.

DOI: 10.1103/PhysRevA.92.053822 PACS number(s): 42.70.Qs, 42.82.Et, 73.43.−f

The creation of topological effects [1] for both electrons [2] and photons [3–17] is of significant current interest. A powerful mechanism for achieving nontrivial topology in a system is to dynamically modulate the system in time. For electrons, such modulation can be achieved by coupling with an external electromagnetic field and has been used to create an electronic Floquet topological insulator [18–23]. For photons, an optical analog of Floquet topological insulators has been demonstrated [24]. Also, time-dependent refractive-index modulations can be used to create an effective magnetic field [25], which can break time-reversal symmetry and create a one-way edge state that is topologically protected against arbitrary disorders.

All previous works on the topological behaviors of dynamically modulated systems have considered only the *weak-coupling* regime, where the modulation strength is far less than the modulation frequency, and have applied the rotating wave approximation (RWA). On the other hand, in recent years, the study of light-matter interactions in the *ultrastrong-coupling* regime, where the RWA is no longer valid, is becoming important [26–33]. It is therefore of fundamental importance to understand topological effects beyond the rotating wave approximation.

In this paper, we analyze a time-dependent Hamiltonian first proposed in Ref. [25] for achieving an effective magnetic field for photons. Unlike Ref. [25], however, here we focus on the ultrastrong-coupling regime where the RWA is no longer valid. Experimentally, reaching such an ultrastrong-coupling regime is in fact relatively straightforward with current photonic technology [34]. For this system in the ultrastrong-coupling regime, we show that the topologically protected one-way photonic edge states can persist over a broad parameter range. Compared with the weak-coupling regime, the topologically protected one-way edge state is less susceptible to intrinsic losses. We also show that, as one varies the modulation strength, there is a topological phase transition that is uniquely associated with the ultrastrong-coupling regime and has no counterpart in weak-coupling systems.

We start with the Hamiltonian [25]

$$H = \omega_A \sum_m a_m^\dagger a_m + \omega_B \sum_n b_n^\dagger b_n + \sum_{\langle mn\rangle} V \cos(\Omega t + \phi_{mn})(a_m^\dagger b_n + b_n^\dagger a_m), \quad (1)$$

which describes a lattice of photonic resonators as shown in Fig. 1. The lattice consists of two sublattices, each consisting of resonators of resonant frequencies ω_A and ω_B, respectively. $a^\dagger$ (a) and $b^\dagger$ (b) are the creation (annihilation) operators associated with the resonators in the two sublattices. The coupling between the resonators are modulated dynamically, where V is the maximum coupling strength, $\Omega = \omega_A - \omega_B$ is the modulation frequency, and ϕ_{mn} is the modulation phase. Such a modulation drives a photonic transition [35] between nearest-neighbor resonators.

Equation (1) can be transformed to the rotating frame with

$$\tilde{a}_m(\tilde{b}_n) = a_m(b_n)e^{i\omega_{A(B)}t}. \quad (2)$$

The Hamiltonian then becomes

$$\tilde{H} = \frac{V}{2}\sum_{\langle mn\rangle}(\tilde{a}_m^\dagger \tilde{b}_n e^{-i\phi_{mn}} + \tilde{b}_n^\dagger \tilde{a}_m e^{i\phi_{mn}} + \tilde{a}_m^\dagger \tilde{b}_n e^{i2\Omega t + i\phi_{mn}} + \tilde{b}_n^\dagger \tilde{a}_m e^{-i2\Omega t - i\phi_{mn}}), \quad (3)$$

where the first two terms define the Hamiltonian $\tilde{H}_{\mathrm{RWA}}$ in the RWA and the last two terms are commonly referred to as the counter-rotating terms.

Reference [25] considered the weak-coupling regime where $V \ll \Omega$ and applied the RWA by ignoring the counter-rotating terms in Eq. (3). In this case, $\tilde{H} \simeq \tilde{H}_{\mathrm{RWA}}$ becomes time independent and is identical to the Hamiltonian of a quantum particle on a lattice subject to a magnetic field described by a vector potential $\boldsymbol{A}$, with $\phi_{mn} = \int_m^n \boldsymbol{A}\cdot d\boldsymbol{l}$ [36]. Such an effective magnetic field provides a new mechanism for controlling the propagation of light [37–40]. In particular, it

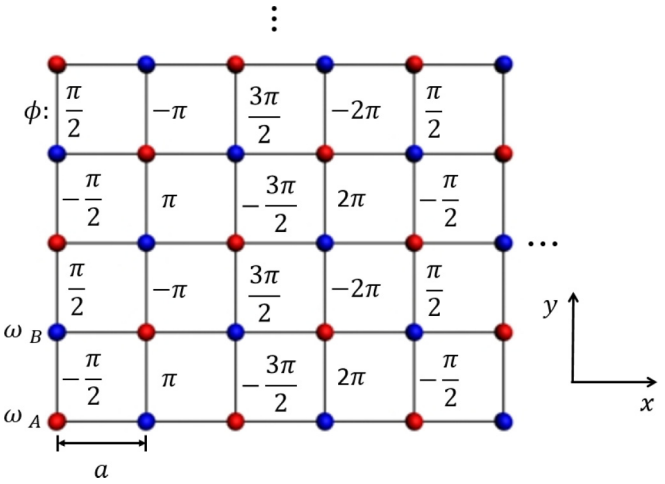

FIG. 1. (Color online) Lattice composed of two types of resonators, A (red) and B (blue). The lines represent coupling (or bonds) between nearest neighbors. All coupling strengths are modulated in time harmonically. For all bonds along the horizontal direction the modulation phase is zero. The bonds along the vertical direction have a spatial distribution of modulation phases as specified in the figure. The specified phases are for the hopping matrix elements of the Hamiltonian in Eq. (1) along the positive y direction.

can be used to achieve a topologically protected one-way edge state [25].

However, from an experimental point of view, it is important to explore the topological behavior of the Hamiltonian of Eq. (1) beyond the weak-coupling regime. The required modulation in Eq. (1) can be achieved electro-optically [34], in which case $V \sim (\delta n/n)\omega_0$, where n is the refractive index, δn is the strength of the index modulation, and ω_0 is the operating frequency. For electro-optic modulation of silicon, to minimize free-carrier loss, $\delta n/n \approx 10^{-5} - 10^{-4}$ [41]. Optical communication typically uses an ω_0 corresponding to a free-space wavelength near 1.5 μm. Thus V is typically between 10–100 GHz. On the other hand, the modulation frequency Ω in electro-optic modulation is also on the order of 10–100 GHz [34]. Thus, experimentally one can readily operate in the regime with $V \sim \Omega$. A similar conclusion can be reached for the acoustic-optical modulation scheme implemented in Ref. [16] for achieving a photonic gauge potential. Unlike the electronic transition, where reaching the ultrastrong-coupling regime is a significant challenge [42–45], for photonic transition [35] it is in fact rather natural that the system operates in the ultrastrong-coupling regime. Thus, systems exhibiting photonic transition can be readily used to explore the physics of ultrastrong coupling.

To explore the topological properties of Eq. (1) in the ultrastrong-coupling regime, we perform a Floquet analysis of the Hamiltonian of Eq. (3). Here we choose a spatial distribution of the modulation phase as shown in Fig. 1. All bonds along the horizontal direction have a zero modulation phase. The bonds along the vertical direction have a spatial distribution of modulation phases. In the weak-coupling regime, such a distribution corresponds to an effective magnetic flux of $\pi/2$, or $1/4$ of the magnetic flux quanta per unit cell. The system is therefore topologically nontrivial in the weak-coupling regime. The aim of the Floquet analysis is then to see to what extent such a nontrivial topological feature persists as one goes beyond the RWA.

Our Floquet band structure analysis follows that of Refs. [46,47]. The system in Fig. 1 is periodic spatially. Therefore the Hamiltonian can be written in the wave-vector space ($\boldsymbol{k}$ space). For each $\boldsymbol{k}$ point, $\tilde{H}$ in Eq. (3) has a period in time $T = \pi/\Omega$. Therefore, the solution of the equation $id/dt|\Psi\rangle - \tilde{H}|\Psi\rangle = 0$ in general takes the form $|\Psi\rangle = e^{-i\varepsilon t}|\Phi\rangle$, where $|\Phi(t+T)\rangle = |\Phi(t)\rangle$ has a periodicity T in time and is commonly referred to as the Floquet eigenstate. ε is the quasienergy and is defined in the temporal first Brillouin zone $\varepsilon \in [-\pi/T, \pi/T] = [-\Omega, \Omega]$. The quasienergies and the Floquet eigenstates can be obtained by solving numerically the eigenvalue equation: $(\tilde{H} - i\partial/\partial t)|\Phi\rangle = \varepsilon|\Phi\rangle$ [46,47]. The quasienergy thus obtained as a function of $\boldsymbol{k}$ defines the Floquet band structure. In the following analysis, we treat both ε and V as a function of Ω.

As an important subtlety, when performing numerical calculation of the Floquet band structures, it is essential to perform a gauge transformation such that the resulting Hamiltonian has the smallest possible temporal period. For our case here, the transformation of Eq. (2), which is a gauge transformation, serves this purpose. While the Hamiltonians H [in Eq. (1)] and $\tilde{H}$ [in Eq. (3)] are equivalent to each other since they are related by the gauge transformation of Eq. (2), the temporal periods of H and $\tilde{H}$ are $2\pi/\Omega$ and π/Ω, respectively. A key aspect of topological band structure analysis is to identify band gaps that are topologically nontrivial. On the other hand, if one analyzes H directly, since the corresponding temporal first Brillouin zone is smaller, there is additional band folding along the quasienergy axis, which obscures the band gap. The use of $\tilde{H}$ in Eq. (3) is in fact quite important for the analysis of the topological aspects of the Floquet band structure.

We now examine the Floquet band structure of the system. $\tilde{H}$ has a spatial periodicity of $4a$ by $2a$ along the x and y directions, respectively. Thus, its Floquet band structure has eight bands, as we can see in Fig. 2.

As a comparison, we first consider the band structure of the Hamiltonian $\tilde{H}_{\mathrm{RWA}}$ as defined by ignoring the counter-rotating terms in Eq. (3). $\tilde{H}_{\mathrm{RWA}}$ has a spatial periodicity of $4a$ by $1a$ along the x and y directions, respectively. However, to facilitate the comparison with the band structure of $\tilde{H}$, here we plot the band structure of $\tilde{H}_{\mathrm{RWA}}$ with the spatial periodicity of $4a$ by $2a$ as well. The resulting RWA band structure, as shown in Fig. 2(a), thus contains eight bands. The bands are twofold degenerate. The band structure has the same shape for different values of V [Fig. 2(a)].

In the RWA band structure, there are two gaps separating the middle group of four bands from the upper and the lower groups, each of two bands, respectively. These gaps are topologically nontrivial, as can be checked by calculating the Chern number [22]:

$$\mathcal{C} = -\frac{1}{2\pi}\sum_{\alpha}\int dk_x dk_y (\nabla_{\vec{k}} \times \mathcal{A}_\alpha), \tag{4}$$

where the summation is over the group of bands, each band indiced by a different α,

$$\mathcal{A}_\alpha = \langle \Phi_\alpha(\vec{k},t)|i\nabla_{\vec{k}}|\Phi_\alpha(\vec{k},t)\rangle. \tag{5}$$

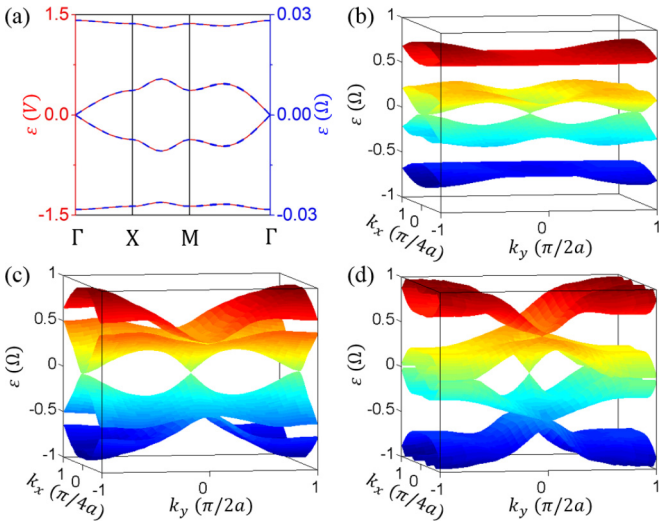

FIG. 2. (Color online) Floquet band structure for the Hamiltonian $\tilde{H}$ of Eq. (3): (a) with RWA from $\tilde{H}_{\mathrm{RWA}}$ (red solid line) and $V = 0.02\Omega$ (blue dashed line), (b) $V = 0.5\Omega$, (c) $V = 1.1\Omega$, and (d) $V = 1.5\Omega$.

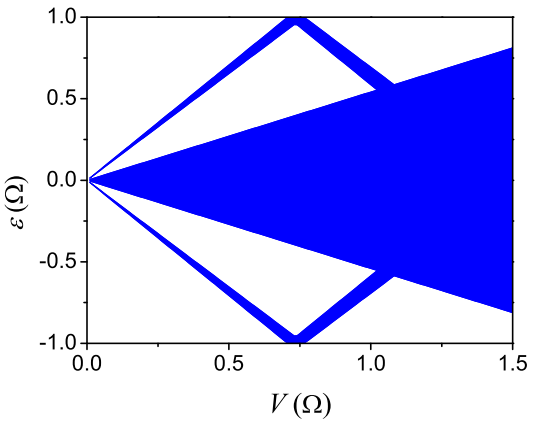

FIG. 3. (Color online) The projected RWA band structure folded into the temporal first Brillouin zone as a function of V. The blue regions correspond to the bands. The white regions are the band gap regions.

The Chern numbers for the upper, middle, and lower groups of bands are $+1$, -2, $+1$, respectively. (As a side note, the middle group of four bands can actually be separated into two subgroups each consisting of two bands, separated by Dirac points at $\varepsilon = 0$. Each of the subgroup has a Chern number -1.) The topological analysis here is consistent with the association of an effective magnetic field in this system. The gaps remain open for all nonzero values of V. Thus with the RWA there is no phase transition as one varies V.

Having reviewed the band structure of $\tilde{H}_{\mathrm{RWA}}$, we now consider the Floquet band structure of the full Hamiltonian $\tilde{H}$. Figure 2(a) shows the cases of $V = 0.02\Omega$; the Floquet band structure $\tilde{H}$ agrees very well with that of the $\tilde{H}_{\mathrm{RWA}}$.

As one increases V to approximately $V > 0.1\Omega$, the RWA is no longer adequate to describe the band structure of $\tilde{H}$. Hence, it is no longer possible to interpret the band structure using the concept of an effective magnetic field. Nevertheless, the two gaps remain open for V ranging from near 0 to 1.1Ω (see Fig. 2). Therefore, in this range of V, the Chern numbers for the upper, middle, and lower groups of bands must remain unchanged at $+1$, -2, $+1$, respectively, and hence the topological aspects of the band structure remain the same as one goes into the ultrastrong-coupling regime.

As V increases from 0, the bands gradually move away from $\varepsilon = 0$ and start to occupy more of the temporal first Brillouin zone [see Fig. 2(b)]. At $V \sim \Omega$, some of these bands reach the edge of the temporal first Brillouin zone. Further increase of V then results in the folding back of these bands back into the temporal first Brillouin zone and the closing of the gaps as we see in Fig. 2(c) with $V = 1.1\Omega$. No gap is found for larger values of V. We see that the increase of V induces a topological phase transition: the system behaves as a Floquet topological insulator at small V and a gapless and topologically trivial "metal" at large V.

The values of V required for achieving such a topological phase transition can be estimated by folding the RWA band structure into the temporal first Brillouin zone of $[-\Omega, \Omega]$ (Fig. 3), which predicts that the gap closes at $V = 1.1\Omega$. In comparsion, for the full Hamiltonian of Eq. (3), the gap actually closes at $V = 1.11\Omega$. Therefore, we see that one can use the RWA to approximately estimate the strength of V at which point the topological phase transition occurs and that this topological phase transition is directly related to the nontrivial topology of the quasienergy space [48]. On the other hand, this calculation again points to the significant difference between the RWA band structure and the actual band structure. For example, while a band gap exists at $V > 1.1\Omega$ for the RWA case, there is no band gap for the actual system at $V > 1.1\Omega$.

A key signature of a topologically nontrivial band gap is the existence of a one-way edge state in a strip geometry. We therefore calculate the projected Floquet band structure for a strip that is infinite in the y direction and has a width of $21a$ in the x direction. The projected band structure consists of the quasienergy of all the eigenstates of the system as a function of k_y. The projected band consists of three groups of bands separated by two topologically nontrivial band gaps. We observe the existence of a one-way edge mode that spans these topologically nontrivial band gaps, as shown in Fig. 4(b) with $V = 0.5\Omega$. Thus the one-way edge state persists in the ultrastrong-coupling regime.

For applications of one-way edge modes to carry information, optimizing the bandwidth of such a one-way edge mode is important. Since the one-way edge mode spans the topologically nontrivial band gap, the size of such a gap becomes a good measure of the bandwidth of the one-way edge mode. In Fig. 4(a), we plot the size of the topologically nontrivial band gap as a function of the modulation strength V. The bandwidth increases with V for small V, peaks at $V = 0.5\Omega$, and then decreases to 0, signifying the topological phase transition mentioned above. For a given modulation frequency Ω, therefore, the bandwidth of the one-way edge mode maximizes at the ultrastrong-coupling regime.

The one-way edge mode is topologically robust against disorder-induced backscattering. However, such a mode is still susceptible to intrinsic losses of the materials. For practical application then mitigation of the effect of intrinsic loss is

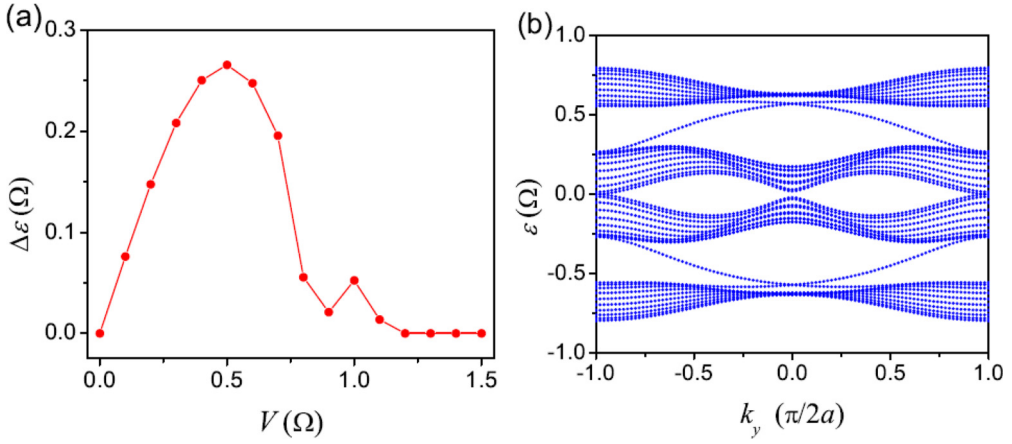

FIG. 4. (Color online) (a) The bandwidth of the topologically nontrivial gap as a function of V. (b) The projected band structure at $V = 0.5\Omega$.

important. For a given modulation frequency Ω, operating in the ultrastrong-coupling regime results in the one-way edge modes that have larger group velocities, and hence are less susceptible to loss, as compared to operating in the weak-coupling regime. As an illustration, we consider a finite structure described by the Hamiltonian of Eq. (1) of a size of $20a$ by $20a$ (Fig. 5). We consider two systems in the weak-coupling and ultrastrong-coupling regimes, corresponding to $V = 0.02\Omega$ and $V = 0.5\Omega$, respectively. To probe the systems, we place a point source at the location $(1a, 10a)$ and choose the frequencies of the point source to be inside one of the topologically nontrivial band gaps ($\omega_s = V$). Both systems indeed support one-way edge modes as shown in Figs. 5(a) and 5(b). To study the effect of loss, we further include in Eq. (1) an extra term, $-i\gamma/2(\sum_m a_m^\dagger a_m + \sum_n b_n^\dagger b_n)$, where

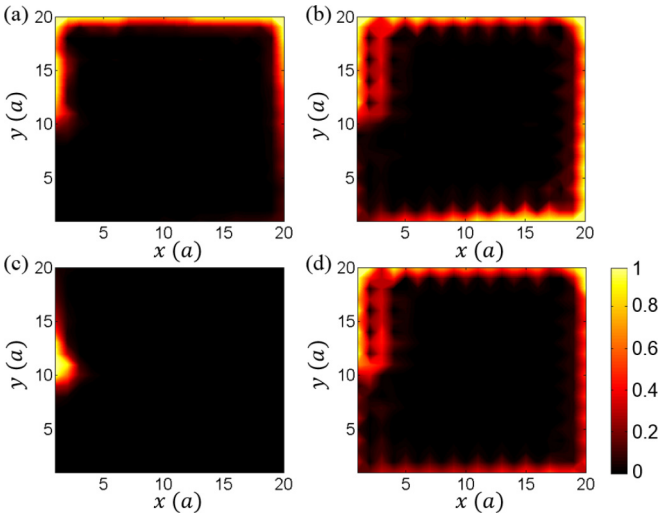

FIG. 5. (Color online) The simulation results with the Hamiltonian (1) in a 20×20 resonator lattice ($\omega_A = 12\pi c/a$, $\omega_B = 0$). A point source is placed at the location (1,10). The propagation field profiles are plotted as follows: (a) at time $t = 100a/c$ with $V = 0.02\Omega$ and the source frequency $\omega_s = V$; (b) at time $t = 10a/c$ with $V = 0.5\Omega$ and $\omega_s = V$; (c) same as panel (a); and (d) same as panel (b) with a loss coefficient $\gamma = 0.2c/a$ at steady state.

$\gamma = 0.2c/a$ is the loss coefficient. The steady-state field distributions for the same source are shown in Fig. 5(c) and 5(d), respectively. We see that the photons indeed have a much longer propagation distance in the ultrastrong-coupling regime with $V = 0.5\Omega$ [Fig. 5(d)], as compared to the weak-coupling regime with $V = 0.02\Omega$ [Fig. 5(c)].

Our numerical treatment with a dissipative system is fully consistent with the standard quantum theory that deals with system-reservoir interactions (see the Appendix for details). The results of our simulation provides the photon distribution function in real space. For the photonic system one is primarily concerned with nonequilibrium transport properties as determined by the edge state. The presented simulation is therefore directly relevant for the experimental study of this system.

In summary, we consider a system of dynamically modulated photonic resonator lattice undergoing photonic transition and show that such a lattice can exhibit nontrivial topological properties in the ultrastrong-coupling regime. From an experimental and practical point of view, for the same modulation frequency, operating the system in the ultrastrong-coupling regime results in a one-way edge mode that has a larger bandwidth, and is less susceptible to loss, as compared to operating the same system in the weak-coupling regime. Our work therefore should provide useful guidance to the experimental quest in seeking to demonstrate topological effects related to time-reversal symmetry breaking on-chip [34]. We also show that in the ultrastrong-coupling regime, the system undergoes a topological phase transition as one varies the modulation strength. This phase transition has no counterpart in weak-coupling systems, and its nature is directly related to the nontrivial topology of the quasienergy space. In the context of recent significant fundamental interest in exploring ultrastrong-coupling physics [26–33,42–45], our work points to the exciting prospect of exploring nontrivial topological effects in ultrastrong-coupling regimes.

This work is supported in part by U.S. Air Force Office of Scientific Research Grant No. FA9550-12-1-0488 and U.S. National Science Foundation Grant No. ECCS-1201914.

APPENDIX

In the simulation procedure that leads to the results in Fig. 5, we introduce an additional non-Hermitian term, $-i\frac{\gamma}{2}(\sum_m a_m^\dagger a_m + \sum_n b_n^\dagger b_n)$, to the Hamiltonian of Eq. (1). We also excite the system by placing a point source at one of the resonators. Here we show that our procedure arises directly from a full quantum mechanical treatment. Specifically, the form of the non-Hermitian term can be obtained by explicitly considered system-reservoir interaction, following the standard procedure in Ref. [49]. Also, the use of a point source is consistent with an input of a coherent state. And as a result our calculation provides a direct treatment of photon distribution function in the presence of a coherent state input.

We consider the Hamiltonian

$$H_{\rm tot} = H + H_R + H_S, \tag{A1}$$

where H is the Hamiltonian of our system which is shown as Eq. (1) in the main text. To introduce loss, we assume that each resonator mode interacts with its own reservoir. The reservoir itself and the system-reservoir interaction is described by

$$\begin{aligned} H_R = &\sum_m \sum_k \omega_k \alpha_{m,k}^\dagger \alpha_{m,k} + \sum_n \sum_k \omega_k \beta_{n,k}^\dagger \beta_{n,k} \\ &+ \sum_m \sum_k g(\alpha_{m,k}^\dagger a_m + a_m^\dagger \alpha_{m,k}) \\ &+ \sum_n \sum_k g(\beta_{n,k}^\dagger b_n + b_n^\dagger \beta_{n,k}). \end{aligned} \tag{A2}$$

Here, $\alpha_{m,k}$ and $\beta_{n,k}$ represent modes in the reservoir coupling to resonator operators a_m and b_n, respectively. The label k forms a one-dimensional continuum, and we assume $\omega_k = c|k|$. g is the resonator-reservoir coupling constant. Here we make the Markovian approximation by assuming that g is independent of k. To describe a coherent state injection at the resonator located at site m_0, we introduce

$$H_S = \omega_S d^\dagger d + \kappa \sum_m (d^\dagger a_m + a_m^\dagger d)\delta_{m,m_0}, \tag{A3}$$

where without loss of generality we assume that the resonator at site m_0 is of the A type. d is the source field operator. ω_S gives the frequency of the source field and κ is the corresponding coupling constant.

We can write the Heisenberg equations of motion for the following operators:

$$\begin{aligned} \dot{a}_m = i[H_{\rm tot}, a_m] = &-i\omega_A a_m - i\sum_{\langle mn\rangle} V\cos(\Omega t + \phi_{mn}) b_n \\ &- i\kappa d\delta_{m,m_0} - i\sum_k g\alpha_{m,k}, \end{aligned} \tag{A4}$$

$$\begin{aligned} \dot{b}_n = i[H_{\rm tot}, b_n] = &-i\omega_B b_n - i\sum_{\langle mn\rangle} V\cos(\Omega t + \phi_{mn}) a_m \\ &- i\sum_k g\beta_{n,k}, \end{aligned} \tag{A5}$$

$$\dot{\alpha}_{m,k} = i[H_{\rm tot}, \alpha_{m,k}] = -i\omega_k \alpha_{m,k} - iga_m, \tag{A6}$$

$$\dot{\beta}_{n,k} = i[H_{\rm tot}, \beta_{n,k}] = -i\omega_k \beta_{n,k} - ig\beta_{n,k}. \tag{A7}$$

Equation (A6) can be integrated as

$$\alpha_{m,k}(t) = \alpha_{m,k}(0)e^{-i\omega_k t} - ig\int_0^t dt' a_m(t')e^{-i\omega_k(t-t')}. \tag{A8}$$

Plugging Eq. (A8) into Eq. (A4), we get

$$\begin{aligned} \dot{a}_m = &-i\omega_A a_m - i\sum_{\langle mn\rangle} V\cos(\Omega t + \phi_{mn}) b_n - i\kappa d\delta_{m,m_0} \\ &- \sum_k g^2 \int_0^t dt' a_m(t')e^{-i\omega_k(t-t')} - i\sum_k g\alpha_{m,k}(0)e^{-i\omega_k t}. \end{aligned} \tag{A9}$$

We do the time integration in Eq. (A9) by replacing $\sum_k$ by $2\frac{L}{2\pi}\int_{-\infty}^{\infty} dk$:

$$\begin{aligned} &\sum_k g^2 \int_0^t dt' a_m(t')e^{-i\omega_k(t-t')} \\ &= 2\frac{L}{2\pi} g^2 \int_0^t dt' a_m(t') \int_{-\infty}^{\infty} dk e^{-i\omega_k(t-t')} \\ &= \frac{g^2 L}{\pi c}\int_0^t dt' a_m(t') 2\pi\delta(t-t') \\ &= \frac{\gamma}{2} a_m(t). \end{aligned} \tag{A10}$$

Here $\gamma \equiv 4g^2 L/c$. Therefore, we obtain the equation of motion for a_m:

$$\begin{aligned} \dot{a}_m = &-\frac{\gamma}{2} a_m(t) - i\omega_A a_m - i\sum_{\langle mn\rangle} V\cos(\Omega t + \phi_{mn}) b_n \\ &- i\kappa d\delta_{m,m_0} - i\sum_k g\alpha_{m,k}(0)e^{-i\omega_k t}. \end{aligned} \tag{A11}$$

Similarly, the equation of motion for b_n is

$$\begin{aligned} \dot{b}_n = &-\frac{\gamma}{2} b_n(t) - i\omega_B b_n - i\sum_{\langle mn\rangle} V\cos(\Omega t + \phi_{mn}) a_m \\ &- i\sum_k g\beta_{n,k}(0)e^{-i\omega_k t}. \end{aligned} \tag{A12}$$

We take the expectation values of Eqs. (A11) and (A12) to arrive at a set of ordinary differential equations. Since optical frequencies correspond to energies that are far higher than the energy scale of room temperature, one can safely assume that $\langle\alpha_{m,k}(0)\rangle_R = \langle\beta_{n,k}(0)\rangle_R = 0$. In addition, we assume that we inject a coherent state at the resonator located at m_0, and therefore, we can replace the operator d by the amplitude s. We therefore arrive at the equations that we used for our simulation:

$$\begin{aligned} \frac{d}{dt}\langle a_m\rangle_R = &-\frac{\gamma}{2}\langle a_m\rangle_R - i\omega_A\langle a_m\rangle_R \\ &- i\sum_{\langle mn\rangle} V\cos(\Omega t + \phi_{mn})\langle b_n\rangle_R - i\kappa s\delta_{m,m_0}, \end{aligned} \tag{A13}$$

$$\begin{aligned} \frac{d}{dt}\langle b_n\rangle_R = &-\frac{\gamma}{2}\langle b_n\rangle_R - i\omega_B\langle b_n\rangle_R \\ &- i\sum_{\langle mn\rangle} V\cos(\Omega t + \phi_{mn})\langle a_m\rangle_R, \end{aligned} \tag{A14}$$

To summarize, as we have shown here, our treatment of the lossy system under coherent state injection is fully consistent with the standard treatment of system-reservoir interaction. The results of the our simulation provide the photon distribution function in real space.

[1] K. V. Klitzing, G. Dorda, and M. Pepper, Phys. Rev. Lett. **45**, 494 (1980).
[2] X.-L. Qi and S.-C. Zhang, Rev. Mod. Phys. **83**, 1057 (2011).
[3] L. Lu, J. D. Joannopoulos, and M. Soljačić, Nat. Photonics **8**, 821 (2014).
[4] F. D. M. Haldane and S. Raghu, Phys. Rev. Lett. **100**, 013904 (2008).
[5] S. Raghu and F. D. M. Haldane, Phys. Rev. A **78**, 033834 (2008).
[6] Z. Wang, Y. Chong, J. D. Joannopoulos, and M. Soljačić, Nature (London) **461**, 772 (2009).
[7] M. Hafezi, E. A. Demler, M. D. Lukin, and J. M. Taylor, Nat. Phys. **7**, 907 (2011).
[8] Y. Poo, R.-X. Wu, Z. Lin, Y. Yang, and C. T. Chan, Phys. Rev. Lett. **106**, 093903 (2011).
[9] S. Liu, W. Lu, Z. Lin, and S. T. Chui, Phys. Rev. B **84**, 045425 (2011).
[10] Y. Poo, R.-X. Wu, S. Liu, Y. Yang, Z. Lin, and S. T. Chui, Appl. Phys. Lett. **101**, 081912 (2012).
[11] M. Hafezi, S. Mittal, J. Fan, A. Migdall, and J. M. Taylor, Nat. Photonics **7**, 1001 (2013).
[12] A. B. Khanikaev, S. H. Mousavi, W.-K. Tse, M. Kargarian, A. H. MacDonald, and G. Shvets, Nat. Mater. **12**, 233 (2013).
[13] S. Longhi, Opt. Lett. **38**, 3570 (2013).
[14] G. Q. Liang and Y. D. Chong, Phys. Rev. Lett. **110**, 203904 (2013).
[15] S. Mittal, J. Fan, S. Faez, A. Migdall, J. M. Taylor, and M. Hafezi, Phys. Rev. Lett. **113**, 087403 (2014).
[16] E. Li, B. J. Eggleton, K. Fang, and S. Fan, Nat. Commun. **5**, 3225 (2014).
[17] A. P. Slobozhanyuk, A. N. Poddubny, A. E. Miroshnichenko, P. A. Belov, and Y. S. Kivshar, Phys. Rev. Lett. **114**, 123901 (2015).
[18] T. Kitagawa, E. Berg, M. Rudner, and E. Demler, Phys. Rev. B **82**, 235114 (2010).
[19] J.-i. Inoue and A. Tanaka, Phys. Rev. Lett. **105**, 017401 (2010).
[20] N. H. Lindner, G. Refael, and V. Galitski, Nat. Phys. **7**, 490 (2011).
[21] A. Gómez-León and G. Platero, Phys. Rev. Lett. **110**, 200403 (2013).
[22] M. S. Rudner, N. H. Lindner, E. Berg, and M. Levin, Phys. Rev. X **3**, 031005 (2013).
[23] J. Cayssol, B. Dóra, F. Simon, and R. Moessner, Phys. Status Solidi RRL **7**, 101 (2013).
[24] M. C. Rechstman, J. M. Zeuner, Y. Plotnik, Y. Lumer, D. Podolsky, F. Dreisow, S. Nolte, M. Segev, and A. Szameit, Nature (London) **496**, 196 (2013).
[25] K. Fang, Z. Yu, and S. Fan, Nat. Photonics **6**, 782 (2012).
[26] E. K. Irish, J. Gea-Banacloche, I. Martin, and K. C. Schwab, Phys. Rev. B **72**, 195410 (2005).
[27] E. K. Irish, Phys. Rev. Lett. **99**, 173601 (2007).
[28] P. Rabl, Phys. Rev. Lett. **107**, 063601 (2011).
[29] M. Schiró, M. Bordyuh, B. Öztop, and H. E. Türeci, Phys. Rev. Lett. **109**, 053601 (2012).
[30] E. Sanchez-Burillo, D. Zueco, J. J. Garcia-Ripoll, and L. Martin-Moreno, Phys. Rev. Lett. **113**, 263604 (2014).
[31] G. Günter, A. A. Anappara, J. Hees, A. Sell, G. Biasiol, L. Sorba, S. De Liberato, C. Ciuti, A. Tredicucci, A. Leitenstorfer, and R. Huber, Nature (London) **458**, 178 (2009).
[32] A. Imamoğlu, Phys. Rev. Lett. **102**, 083602 (2009).
[33] T. Niemczyk, F. Deppe, H. Huebl, E. P. Menzel, F. Hocke, M. J. Schwarz, J. J. Garcia-Ripoll, D. Zueco, T. Hümmer, E. Solano, A. Marx, and R. Gross, Nat. Phys. **6**, 772 (2010).
[34] L. D. Tzuang, K. Fang, P. Nussenzveig, S. Fan, and M. Lipson, Nat. Photonics **8**, 701 (2014).
[35] J. N. Winn, S. Fan, J. D. Joannopoulos, and E. P. Ippen, Phys. Rev. B **59**, 1551 (1999).
[36] R. E. Peierls, Z. Phys. **80**, 763 (1933).
[37] K. Fang and S. Fan, Phys. Rev. Lett. **111**, 203901 (2013).
[38] K. Fang, Z. Yu, and S. Fan, Opt. Express **21**, 18216 (2013).
[39] Q. Lin and S. Fan, Phys. Rev. X **4**, 031031 (2014).
[40] L. Yuan and S. Fan, Phys. Rev. Lett. **114**, 243901 (2015).
[41] M. Lipson, J. Lightwave Technol. **23**, 4222 (2005).
[42] G. Scalari, C. Maissen, D. Turčinková, D. Hagenmüller, S. De Liberato, C. Ciuti, C. Reichl, D. Schuh, W. Wegscheider, M. Beck, and J. Faist, Science **335**, 1323 (2012).
[43] M. Geiser, F. Castellano, G. Scalari, M. Beck, L. Nevou, and J. Faist, Phys. Rev. Lett. **108**, 106402 (2012).
[44] J. Li, M. P. Silveri, K. S. Kumar, J.-M. Pirkkalainen, A. Vepsäläinen, W. C. Chien, J. Tuorila, M. A. Sillanpää, P. J. Hakonen, E. V. Thuneberg, and G. S. Paraoanu, Nat. Commun. **4**, 1420 (2013).
[45] G. Scalari, C. Maissen, S. Cibella, R. Leoni, P. Carelli, F. Valmorra, M. Beck, and J. Faist, New J. Phys. **16**, 033005 (2014).
[46] J. H. Shirley, Phys. Rev. **138**, B979 (1965).
[47] H. Samba, Phys. Rev. A **7**, 2203 (1973).
[48] The quasienergy space has a homotopy group of Z, whereas the standard energy space has a trivial homotopy group. For further discussions of homotopy groups, see M. Nakahara, *Geometry, Topology and Physics*, 2nd ed. (Institute of Physics Publishing, Bristol, 2003).
[49] M. O. Scully and M. S. Zubairy, *Quantum Optics* (Cambridge University Press, Cambridge, UK, 1997), p. 271.